



Hybrid sol-gel coatings applied on anodized AA2024-T3 for active corrosion protection

R. del Olmo^{a,1}, U. Tiringier^{b,*}, I. Milošev^c, P. Visser^d, R. Arrabal^a, E. Matykina^a, J.M.C. Mol^b

^a Departamento de Ingeniería Química y de Materiales, Facultad de Ciencias Químicas, Universidad Complutense, 28040 Madrid, Spain

^b Delft University of Technology, Department of Materials Science and Engineering, Mekelweg 2, 2628 CD Delft, the Netherlands

^c Department of Physical and Organic Chemistry, Jozef Stefan Institute, SI-1000 Ljubljana, Slovenia

^d AkzoNobel, Research & Development, Rijksweg 31, Sassenheim 2171 AJ, the Netherlands

ARTICLE INFO

Keywords:

AA2024-T3

Anodizing

Sol-gel coating

Corrosion inhibitor

Active corrosion protection

ABSTRACT

The effect of the presence of an anodic film and hybrid sol-gel coating loaded with corrosion inhibitors was evaluated as a strategy for enhanced barrier and active corrosion protection of aluminium alloy 2024-T3. In this study, AA2024-T3 specimens were anodized in a modified sulphuric-citric acid bath (SCA) as the first layer of a corrosion protective multilayer system and subsequently protected by the application of silica-based hybrid sol-gel coatings. These coatings were doped with LiNO_3 and $\text{Ce}(\text{NO}_3)_3$ as corrosion inhibitors and studied in comparison with the inhibitor-free sol-gel coating in terms of morphology, composition and corrosion protection of intact and scribed specimens. The anodized AA2024-T3 with an overlaying inhibitor-free sol-gel coating showed the highest impedance modulus during long-term immersion in $0.1 \text{ mol}\cdot\text{L}^{-1}$ NaCl aqueous solution. Active corrosion protection of scribed coated specimens was studied by exposure to a $0.5 \text{ mol}\cdot\text{L}^{-1}$ NaCl solution and evaluated by surface analytical techniques. The addition of Li- and Ce-based salts into the hybrid sol-gel formulation showed active corrosion protection compared to the inhibitor-free scribed hybrid sol-gel coating. The Ce-doped sol-gel coating showed less visual corrosion and higher active corrosion protection than the Li-containing one during the long-term immersion test in $0.5 \text{ mol}\cdot\text{L}^{-1}$ NaCl. Present findings reveal that the combination of the anodic/hybrid sol-gel layers on AA2024-T3 enhances the corrosion protective properties barrier properties of both stand-alone systems and the incorporation of Li- and Ce-based inhibitors provide active corrosion.

1. Introduction

AA2024-T3 is one of the most commonly used aluminium alloys (AAs) in the aircraft industry due to its low density and high strength-to-weight ratio. The microstructure of AA2024-T3 is complex, comprising a relatively high density and wide variety of intermetallic particles, which enhances its inherent corrosion susceptibility [1]. For this reason, AA2024-T3 is typically surface treated in a multistep surface protection scheme according to strict aerospace regulations, including anodizing and sealing post-treatments [2]. Traditionally, hexavalent chromium based chemistries have been used in both pre-treatment processes (anodizing and chemical conversion coating) and primer coating systems and have shown to provide effective corrosion protection of aluminium alloys for many years [3–8]. However, given its intrinsic

health and safety issues coming along with it, the use of toxic hexavalent chromium is aimed to be substituted by eco-friendly alternatives with urgency [4,9,10]. For this reason, numerous studies on the replacement of hexavalent chromium based chemistries in corrosion protection schemes are being carried out over the last decades [11,12].

One of the promising replacements for chromic acid anodizing (CAA) for corrosion protection is sulphuric acid anodizing (SAA) [4,13]. SAA is widely utilized for corrosion protection of aluminium alloys, including AA2024-T3 in non-painted and painted conditions [4]. However, the typical SAA layer thickness is approximately $10\text{--}20 \mu\text{m}$, which is higher compared to that for the CAA layer ($2\text{--}7 \mu\text{m}$), resulting in a reduction of fatigue strength [4,14,15].

Recently, thin sulphuric acid anodizing (TSAA) has been introduced as a potential alternative to CAA for niche applications to obtain a

* Corresponding author.

E-mail address: U.Tiringier-1@tudelft.nl (U. Tiringier).

¹ These authors have equally contributed to this work.

thinner layer ($\sim 3 \mu\text{m}$) and fulfil the strict fatigue requirements in the aircraft industry [13,16]. The main drawback of TSAA is its lower corrosion resistance compared to SAA, which is a result of their porous morphology and their relatively low thickness [4,13,16]. A promising way to overcome this limitation and promote the formation of protective anodic films with improved corrosion resistance is the incorporation of carboxylic acids (e.g. tartaric, citric, glycolic, oxalic, malonic, etc) in the electrolyte bath [14,17–20]. Among the different additives, several authors confirmed the positive corrosion protection effect of tartaric and citric acids in the TSAA bath since inhibiting anodic oxide layer dissolution in corrosive environments due to their incorporation in the anodic film surface [20,21]. This approach is environmentally friendly and provides superior surface finishing, process stability and enhanced corrosion protection compared to stand-alone TSAA [17–19,22]. However, their corrosion protective performance is still not comparable with CAA. Therefore, an additional sealing post-treatment is required.

On that basis, sol-gel coatings are one of the promising candidates for sealing [11] since actual hexavalent-chromium-free sealing alternatives do not meet the corrosion protection requirements in the aircraft industry [9,14,15]. Sol-gel technology offers several advantages, such as cost-effectiveness and simple application procedures [23–25]. The early sol-gel coating types were based on inorganic silane precursors, which offer good mechanical properties and promote good adhesion between the metal substrate, leading to low oxygen diffusion [26]. However, they contain micropores and microcracks and require a relatively high curing temperature, from 400 to 800 °C [24].

Hybrid sol-gel coatings (HSG) were developed in the early nineteen-eighties as promising replacements for toxic chromate conversion coatings [11]. They are prepared with a combination of inorganic and organic precursors, where the organic part enables low-temperature curing, $<150^\circ\text{C}$ [24,27,28], and improves mechanical properties (flexibility), thus increasing their ability to comply with the requirements of the aircraft industry [28,29].

HSG coatings provide barrier corrosion protection to aluminium alloys but do not provide active corrosion protection when damage occurs. Corrosion inhibitors, such as Ce-based salts may be incorporated into the sol-gel coatings to enhance their active corrosion protective properties [30,31].

When corrosion occurs, reduction of oxygen takes place at the cathodic sites of the aluminium alloy microstructure, OH^- ions are formed and pH increases at these local cathodic sites. Ce^{3+} ions hydrolyse and cerium (III) hydroxide ($\text{Ce}(\text{OH})_3$) precipitates at the cathodic sites at the surface of AA2024-T3. $\text{Ce}(\text{OH})_3$ formed can be further oxidized to more stable $\text{Ce}(\text{OH})_4$ and insoluble CeO_2 , which acts as a protective barrier to oxygen and lowers the cathodic activity by hindering the transfer of electrons from the anodic to cathodic sites [32–35].

Moreover, the addition of trivalent cerium chemistries into the hybrid sol-gel coating has also provided a self-healing capability to the coating [11]. It was confirmed that $\text{Ce}(\text{NO}_3)_3$ favours the condensation and polymerization of both inorganic and organic networks of the HSG coating, which results in enhanced corrosion protection as compared to that for stand-alone HSG coatings [36].

Another class of corrosion inhibitors for aluminium alloys is lithium-based salts [37–41]. They became of interest as potential corrosion inhibitors after reports of enhanced passivity of aluminium when it is exposed to alkaline lithium salt solutions, such as Li_2CO_3 [11,42,43]. Lithium-ions can leach from the organic coating and generate a protective layer in the damaged area [38,40,44]. More recently, Trentin et al. [45] studied the effect of LiCO_3 in hybrid sol-gel coatings and observed an improvement in the polymerization efficiency by a reduction of stacking defects. Besides, the self-healing ability of these compounds was observed by the formation of a protective layer of lithium-containing (hydr)oxides at local defects [36].

Based on the explained above, inhibitor-doped HSG can be a potential sealing method after anodizing, since it may offer various

advantages, such as barrier and active corrosion protection. Nevertheless, literature based on the concept of duplex coatings based on anodic film/HSG systems is limited [46–48] but, significant corrosion improvement is achieved compared to stand-alone sol-gel or anodic layers. So far, the concept of stand-alone and Ce-doped HSG coatings has been evaluated for conventional tartaric-sulphuric (TSA) and thick sulphuric acid-based (SAA) films providing a significant corrosion protection performance [46,47,49].

However, there is a lack of understanding of how a modified-TSAA layer influences HSG performance in terms of coating morphology, corrosion resistance and active protection ability when it is doped with corrosion inhibitors.

In the present study, these aspects are investigated using three silane-based HSG coatings (stand-alone and doped with Li and Ce salts) based on inorganic tetraethyl orthosilicate (TEOS) and (3-Glycidyloxypropyl)trimethoxysilane GPTMS.

HSG coatings were deposited on citric acid-containing TSAA anodized AA2024-T3 (previously selected after a screening process) by the dip-coating technique. To evaluate the role of the anodic film before and after sol-gel deposition, coating morphology, composition and corrosion properties were studied with the following techniques: scanning electron microscopy equipped with energy-dispersive X-ray spectroscopy (SEM/EDS), eddy-current thickness measurement, electrochemical impedance spectroscopy (EIS) and digital optical microscopy. To evaluate active corrosion protection of different coatings, specimens were scribed and the differences of the scribe for different coatings were monitored during immersion time in terms of morphology and electrochemical properties.

2. Experimental methods

2.1. Specimens preparation

Substrates used in the present work are aluminium alloys AA2024-T3, supplied by Kaiser Aluminum (Table 1) [50].

The size of substrates was $40 \text{ mm} \times 25 \text{ mm} \times 2 \text{ mm}$ and they were cleaned in 70 g L^{-1} BONDERITE C-AK 4215NC solution for 10 min at 60°C and etched in 85 g L^{-1} BONDERITE C-AK ALUM ETCH 2 AERO at 40°C for 2 min. Each procedure was followed by rinsing in deionized water. Finally, specimens were desmutted by immersion in BONDERITE C-IC SMUTGO NC AERO for 5 min, rinsed in deionized water and dried with warm air. The working area for anodizing treatment was $\sim 20 \text{ cm}^2$ with an electrical connection provided through a shielded copper wire.

2.2. Anodizing process

Anodic films were obtained in 3 different electrolytes (Table 2) according to the MIL-A-8625F specification for type IIB coatings for TSAA and SCA electrolytes [16,51]. Anodizing conditions of the TSA process were established considering previous studies and commonly used industrial conditions [4,52,53]. The experimental system was equipped with a double-walled glass cell to keep the electrolyte temperature under continuous electrolyte agitation. The anodic films were formed using a DC power supply (SM120-AR-8 Systems electronic) and a commercially pure aluminium plate was used as a counter electrode. After anodizing, specimens were rinsed with deionized water and dried with a stream of air. All specimens were tested in duplicate.

2.3. Hybrid sol-gel synthesis

Three HSG coatings were prepared in the present work, the first without corrosion inhibitor as a reference, the second doped with $\text{Ce}(\text{NO}_3)_3 \cdot 6 \text{ H}_2\text{O}$ and the third with LiNO_3 as corrosion inhibitors. First, stand-alone hybrid sol-gel coatings were prepared by mixing tetraethoxysilane (TEOS, Aldrich, 99%), 3-(glycidyloxypropyl)trimethoxysilane (GPTMS, ABCR, 98%) and colloidal silica SiO_2 (Ludox-4S,

Table 1

Chemical composition of aluminium alloy 2024-T3.

Alloy	Elements (wt%)								
	Cu	Mg	Mn	Fe	Si	Zn	Ti	Cr	Al
AA2024-T3	3.8–4.9	1.2–1.8	0.3–0.9	<0.5	<0.5	<0.25	<0.15	<0.10	Balance

Table 2

Anodizing treatments evaluated for HSG deposition.

Anodic film	Electrolyte composition (mol L ⁻¹)	Voltage (V)/slope (V min ⁻¹)	Temperature (°C)
TSAA	- H ₂ SO ₄ (sulphuric acid): 1.5	15/5	25 ± 1
SCA	- H ₂ SO ₄ (sulphuric acid): 1.5 - C ₆ H ₈ O ₇ (citric acid): 0, 0.1, 0.25 and 0.5	15/5	25 ± 1
TSA	- C ₄ H ₆ O ₆ (tartaric acid): 0.5 - H ₂ SO ₄ (sulphuric acid): 0.5	14/2.8	37 ± 1

Aldrich, aqueous suspension 40 wt%). After 30 min of stirring, the hydrolysis was completed and 0.6 mL of concentrated HNO₃ (VWR, 65%) was added as a catalyst for polycondensation and the solution was stirred for 5 min. Finally, absolute ethanol was added as a solvent. The molar ratio of the first sol was TEOS/GPTMS/SiO₂ = 0.5/0.5/0.54, denoted as GTS. The inhibitor-containing HSG coatings were prepared in the same way, just by using Li(NO₃)₃ and Ce(NO₃)₃·6 H₂O salts as corrosion inhibitors, respectively. The molar ratio of the second sol was TEOS/GPTMS/SiO₂/Li = 0.5/0.5/0.54/0.03, denoted as GTS-Li and the third sol was TEOS/GPTMS/SiO₂/Ce = 0.5/0.5/0.54/0.03, denoted as

GTS-Ce.

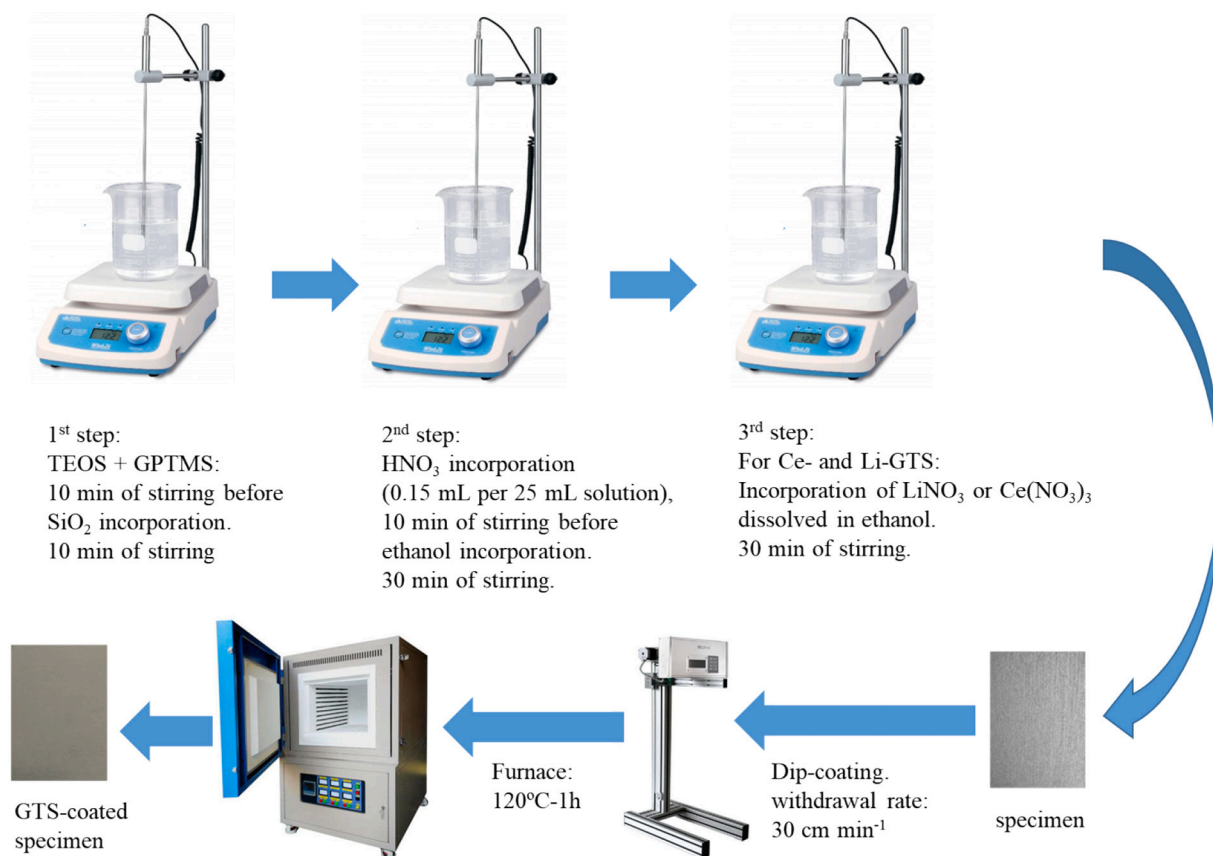
All HSG coatings (GTS, GTS-Li and GTS-Ce) were deposited on previously anodized (SCA) AA2024-T3 by dip-coating technique, with a withdrawal rate of 30 cm min⁻¹. The residence time of the samples in the solution was 1 s. Samples were heat-treated for 1 h at 120 °C to complete the polymerization between the sol and the substrate. The designation of the final duplex coatings was the following: SCA-GTS, SCA-GTS6-Li and SCA-GTS-Ce. The schematic of the synthesis steps is presented in Fig. 1.

2.4. Coating and performance analysis of intact samples

The anodic films with and without HSG coatings were evaluated by scanning electron microscopy equipped with energy-dispersive X-ray spectroscopy and electrochemical impedance spectroscopy.

2.5. Coating characterization

The surface morphology and composition of all studied specimens were obtained by JEOL IT100 Scanning Electron Microscope (SEM), coupled with an energy dispersive spectrometry (EDS) analyzer. Images were recorded in a compositional mode using an accelerating voltage of 10 kV and a working distance of 11 mm. All measurements were performed in a low vacuum mode because of the non-conductive nature of sol-gel coatings. Data were processed with InTouchScope™ software.

**Fig. 1.** Hybrid sol-gel route scheme for selected anodized specimen on AA2024-T3.

Coating thicknesses of the studied specimens were determined in triplicate using an eddy-current meter ISOSCOPE FMP10 (Fischer) equipped with an FTA3.3H probe.

2.6. Electrochemical impedance spectroscopy

Electrochemical impedance spectroscopy (EIS) was used to evaluate the corrosion protection provided by the anodic films-HSG coatings in an aqueous saline solution (0.1 mol L^{-1} NaCl), at room temperature for up to 28 days. Specimens with an exposed area of $\sim 1 \text{ cm}^2$ were placed in a three-electrode cell, connected to a Biologic VMP-300 multichannel potentiostat computer-controlled by EC-Lab software. Silver-silver chloride (Ag/AgCl , 3 M KCl) was used as a reference electrode (0.192 V vs. standard hydrogen electrode), while a steel rod was used as a counter electrode. A sinusoidal perturbation of 10 mV was applied in the frequency range of 10^5 – 10^{-2} Hz .

The goodness of fit was ensured through chi-squared values < 0.01 (square of the standard deviation between the original data and the calculated spectrum). The obtained errors for the individual parameters of the equivalent electrical circuits were $< 5\%$. All specimens were tested in duplicate.

2.7. Active corrosion protection analysis of scribed samples

To evaluate the active corrosion protection ability of the anodic films-HSG coatings with and without inhibitor, they were manually scribed with a standard zirconia tip across the sample surface (a cross-shaped scribe, with a width of 0.1 mm and a length of 2 cm ; the depth of the scribe was larger than the coating thickness and reached the underlying substrate). Hereafter, the scribed samples were exposed to 0.5 mol L^{-1} NaCl solution for 48 h to accelerate the corrosion process.

The visual changes on the coating and inside the scribe were monitored using a digital microscope (Keyence VHX-100) equipped with an 18 megapixel CCD camera, for 21 days of exposure to a 20 mL of 0.5 mol L^{-1} naturally aerated NaCl solution. The magnification ($250\times$) and light conditions were controlled and kept constant throughout the experiment. To obtain compositional changes in the scribe area, SEM/EDS analysis was carried out.

3. Results and discussion

3.1. Anodic film screening

Screening of the TSAA, modified TSAA and TSA anodic films with and without HSG sealing was conducted according to the modulus of impedance at low frequency ($|Z|$ at 10^{-2} Hz) in 0.1 mol L^{-1} NaCl after 1 h of immersion. The best candidates had to combine uniform surface appearance and the highest impedance modulus. Different corrosion protection responses were obtained depending on the used carboxylic acid and more specifically, the concentration of citric acid (Fig. 2). On that basis, TSAA doped with 0.25 M of citric acid showed the best corrosion performance.

Contrarily to the other studied additives, citrate anions are known to form an insoluble salt with aluminium, which may be responsible for the enhanced corrosion resistance. Something similar has been proposed for tartrate ions. According to other studies, insoluble aluminium tartrate may already form during the rinsing step after anodizing due to the increased pH within the pores [53]. However, there is no direct evidence of such product [54–56]. Note that chemical databases indicate that aluminium citrate is slightly less soluble in water than aluminium tartrate [57] suggesting that it is more protective.

The lower corrosion protection provided at 0.5 M of citric acid may be related to the increased field-assisted dissolution due to the higher dissolving power of the electrolyte. At 0.1 M of citric acid, the formation of solid products and complexes was not highly favoured [21].

For this reason, SCA-0.25 M (from now on SCA) was selected due to

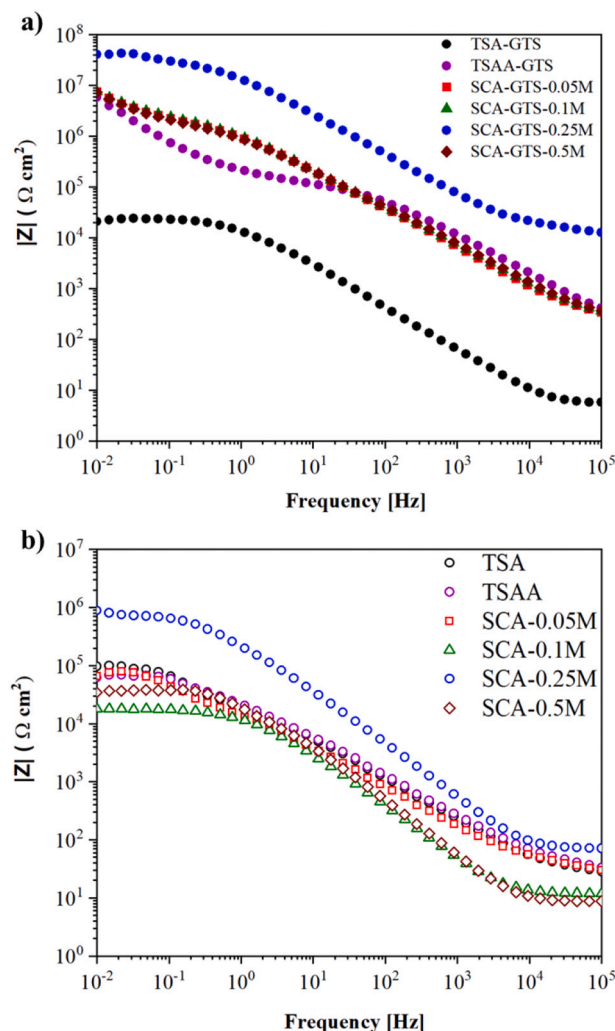


Fig. 2. Bode plots of the studied SCA anodic film (a) with and (b) without GTS coating after 1 h of immersion in 0.1 mol L^{-1} NaCl solution.

its higher corrosion resistance with and without HSG coating for further HSG characterization, detailed corrosion performance study and active protection testing.

3.2. Characterization and corrosion performance analysis of intact samples

3.2.1. SCA and SCA-HSG coatings characterization

Fig. 3 shows the top view scanning electron micrographs of SCA, SCA-GTS, SCA-GTS-Li and SCA-GTS-Ce coatings. The surface of SCA (Fig. 3a) exhibits a typical TSAA layer morphology with visible rolling lines and randomly distributed scallops due to the dissolution of inter-metallic compounds from the AA204-T3 surface (mainly S-phase particles, Al_2CuMg) (Fig. 3b) at the early stages of the anodizing process [14,58,59]. Several authors reported that copper gets incorporated into the anodic film, promoting the generation of oxygen gas during the anodizing process and a highly tortuous pore network, better known as lateral porosity [60,61]. EDS analysis at different locations (marked as 3 in Fig. 3) shows the usual elements found on TSAA films on Al-Cu-Mg alloys, such as Cu, Mg and S [17,62].

Studied SCA-GTS and SCA-GTS-Ce coatings showed a similarly smooth homogeneous morphology (Fig. 3c–h). This indicates a sound interaction between inorganic (SiO_2) and organic (TEOS and GPTMS) components [63,64]. In the case of the SCA-GTS-Ce specimen, Ce^{3+} cations tend to promote the condensation and polymerization of both

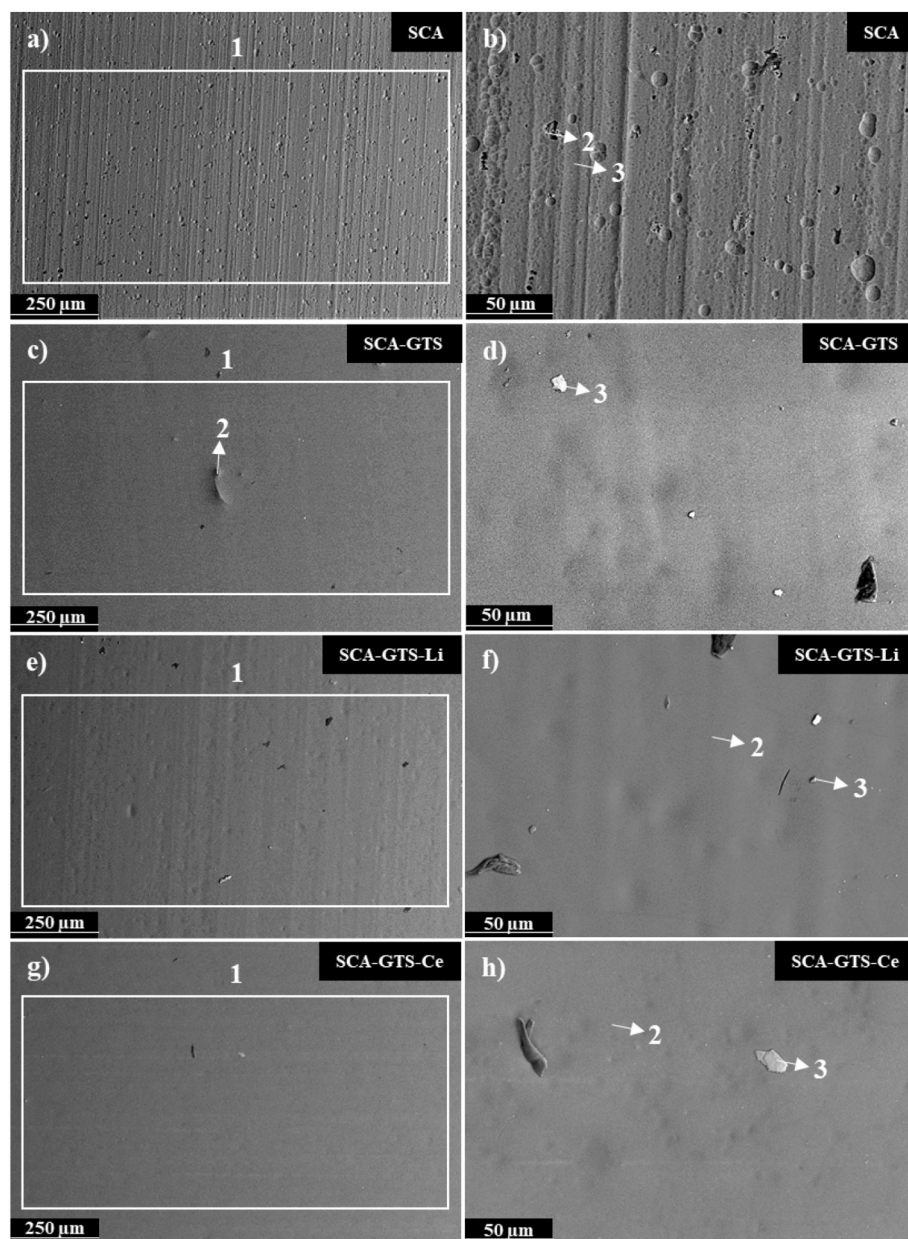


Fig. 3. Top-view scanning electron micrographs of (a, b) stand-alone SCA anodic film and SCA/HSG duplex coatings: (c, d) SCA-GTS; (e, f) SCA-GTS-Li; and (g, h) SCA-GTS-Ce.

inorganic and organic GTS networks on SCA film was confirmed. Conversely, the SCA-GTS-Li specimen was almost transparent and exhibited rolling patterns and scallops of the underlying anodic film (Fig. 3e, f), which could be due to its relatively low thickness in comparison to SCA-GTS and SCA-GTS-Ce coatings. According to the present findings, lithium addition may have a detrimental effect on the condensation of the studied GTS formulation and the resulting GTS-Li film thickness.

The EDS analysis of the studied HSG coatings reveals that the surface is composed mainly of C, O, and Si (Table 3). This is in accordance with previous studies [48,64].

Some Al and Mg from SCA anodic film were incorporated in both SCA-GTS (Fig. 3c, d; Table 3) and SCA-GTS-Ce coatings (Fig. 3g, h; Table 3). This is usually associated with interfacial diffusion processes during the curing step of HSG coatings, thereby denoting an optimal interaction between the HSG coating and the substrate [47,49,65,66], i. e. SCA film. Regarding SCA-GTS-Li coating, Al and Mg were not detected

Table 3

EDS analysis of the SCA, SCA-GTS, SCA-GTS-Li and SCA-GTS-Ce coatings (at.%). Locations are denoted on SEM images in Fig. 3.

Coating	Location	C	O	Mg	Al	S	Cu	Si
SCA	1	5.6	58.9	0.4	31.5	3.2	0.4	
	2	4.5	60.1		32.1	3.3		
	3	3.5	60.5	0.4	32.3	3.3		
SCA-GTS	1	37.1	47.3		0.5			15.1
	2	34.3	48.7		0.4			16.6
	3	22.0	54.4	6.2	0.6			16.8
SCA-GTS-Li	1	36.3	47.5					16.2
	2	34.7	48.5					16.8
	3	34.5	48.4					17.1
SCA-GTS-Ce	1	37.1	46.8					16.1
	2	32.5	49.6		0.2			17.7
	3	24.1	53.1	7.3				15.5

(Fig. 3e, f; Table 3). This may be related to the low diffusion of Al throughout the HSG coating, corresponding to a lesser interaction of the Li-containing GTS coating to the SCA anodic film [45,67].

It is interesting to note that Li or Ce were not detected by the EDS analysis (Table 3). For Li, this is due to its low atomic number, which makes it undetectable by SEM/EDS analysis [37,38,40]. The exact reason for this preferential incorporation has been previously associated with the possible precipitation of cerium-containing nanoparticles within the coating structure [68]. In this case, it could be related to the homogeneous Ce incorporation in the inner GTS coatings part since the Ce content in the sol-gel formulation (0.8 wt%) is superior to the detection limit of the EDS analysis (detection limit: 0.01 wt%) [69].

The resulting coating thickness measurements of the studied SCA anodic film was $4.5 \pm 0.2 \mu\text{m}$. After GTS sealing, the studied coatings reveal thicker values for SCA-GTS ($6.5 \pm 0.2 \mu\text{m}$) and SCA-GTS-Ce ($6.5 \pm 0.2 \mu\text{m}$) coatings and slightly thinner for SCA-GTS-Li ($5.5 \pm 0.3 \mu\text{m}$).

3.2.2. Corrosion protection of SCA and SCA-HSG coatings

Fig. 4 shows the Bode and Nyquist plots obtained for the studied specimens, after 1 h and 28 days of immersion in 0.1 mol L^{-1} NaCl solution.

The presence of different relaxation processes can be observed in the Bode plots of all studied specimens. Three distinct regions are evident: (i) high frequency range (10^3 – 10^5 Hz) related to the outer part of the coating at the coating/electrolyte interface, (ii) intermediate frequency range (10^0 – 10^2 Hz) related to the intermediate hybrid anodic-HSG layer and (iii) low frequency range (10^{-2} Hz) related to charge transfer processes at the inner metal/barrier layer interface, providing an estimation of the overall corrosion resistance, where higher values of $|Z|$ indicate a lower corrosion rate [46,47,70].

For short immersion time (1 h), the impedance modulus response of SCA (Fig. 4a) revealed two relaxation processes related to the response of the outer porous layer (medium/high frequencies) and the barrier layer of the anodic film (low frequency) [47]. The impedance modulus

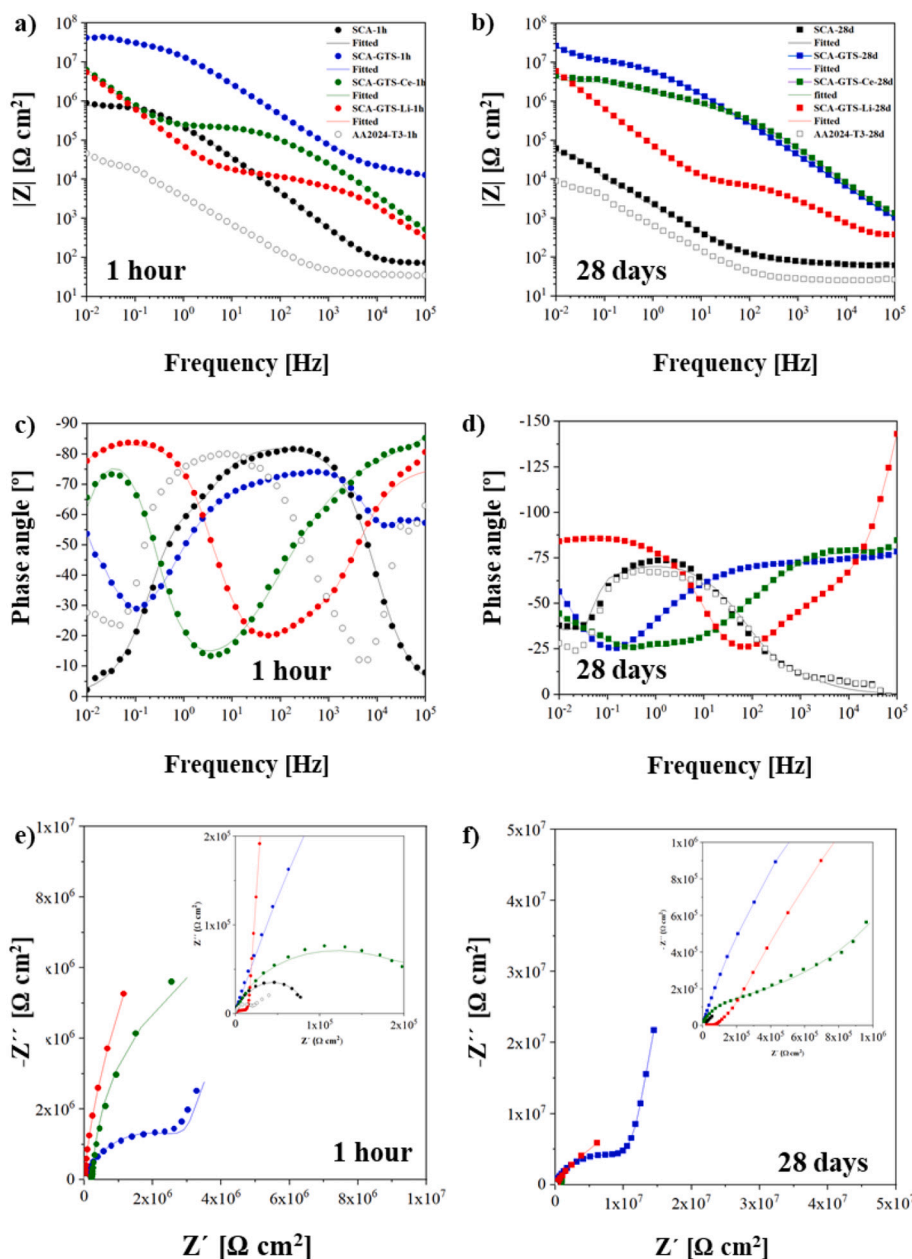


Fig. 4. Bode (a–d) and Nyquist (e–f) plots of all studied samples after (a, c, e) 1 h and (b, d, f) 28 days for bare AA2024-T3, stand-alone SCA and SCA-GTS coatings in 0.1 mol L^{-1} NaCl solution.

at 10^{-2} Hz of SCA film was about one order of magnitude higher than that for the bare AA2024-T3 substrate and one magnitude order lower compared to SCA-GTS, SCA-GTS-Ce and SCA-GTS-Li, showing the corrosion resistance improvement after the HSG application on the SCA layer [46,47].

The impedance modulus for the entire frequency range for SCA-GTS was higher than that for SCA-GTS-Ce and SCA-GTS-Li, respectively (Fig. 4a). This suggests both Ce- and Li-based salts may affect internal stress, as other studies stated [45,71]. More specifically, in the case of Ce, this finding is in accordance with Tiringer et al. [71], who confirmed enhanced barrier properties of stand-alone GTS compared to GTS-Ce coating on 7075 aluminium alloys. However, in the phase angle-frequency plots (Fig. 4c), higher angle values at high frequencies (10^3 – 10^5) were achieved for SCA-GTS-Li and SCA-GTS-Ce coatings, thereby indicating their higher stability compared to the SCA-GTS coating [46,47]. The drop in the phase angle in the mid frequency range (observed in Fig. 2c) can be attributed to the diffusion of corrosive species. This was likewise confirmed in Nyquist plots (Fig. 4e) since the slopes of SCA-GTS-Li and SCA-GTS-Ce coatings were higher in the whole frequency range in comparison to that of the SCA-GTS coating [72].

After 28 days of immersion, GTS-coated specimens show a negligible decrease of the impedance modulus at low frequency in comparison to stand-alone SCA film (Fig. 4b) indicating the beneficial effect of GTS coating in long-term corrosion resistance [73]. The phase angle values at high frequency were higher for SCA-GTS-Li and SCA-GTS-Ce coatings compared to those for SCA-GTS specimen, indicating that the electrolyte hardly penetrates across the coating structure (Fig. 4d) [45,71]. However, at low frequencies, the phase angle value of SCA-GTS and SCA-GTS-Ce specimens was lower. This is usually attributed to their higher protective sol-gel response, indicating the increased mobility of the corrosive ions within the layer [47,74].

By way of comparison between SCA-GTS and inhibitor-containing SCA-GTS coatings, the presence of a semicircle in the Nyquist plot of SCA-GTS coating (Fig. 4f) is associated with higher coating degradation [72]. In the case of SCA-GTS-Li and SCA-GTS-Ce coatings, the diffusion processes observed at low frequencies can also be related to the electrolyte penetration throughout the coating structure (Fig. 4f). This may be related to the corrosion protective character of the stand-alone HSG coating and/or additional factors such as the formation of protective corrosion products after the long-term corrosion process [45].

To further investigate the corrosion performance of studied specimens, equivalent circuits were used to fit the experimental data after 1 h (Fig. 5, Table 4) and 28 d of immersion time (Fig. 6, Table 4). In all circuits, R_{sol} accounts for the resistance of the electrolyte and constant phase elements (CPE) were used instead of capacitances to account for

the non-ideal behavior of the system [11].

After 1 h of immersion of stand-alone SCA anodic film, CPE_{por}/R_{por} are ascribed to the outer porous layer and CPE_b/R_b to the barrier layer (Fig. 5a) [49,75]. For SCA-GTS duplex coatings, CPE_{GTS}/R_{GTS} represent the outer sol-gel coating and CPE_{hl}/R_{hl} the mixed anodic/sol-gel layer (Fig. 5b) [46,73]. The incorporation of Ce and Li into the GTS formulation resulted in lower R_{GTS} , R_{hl} and R_b values in comparison to SCA-GTS coating (Table 4). It could be related to the higher coating thickness of the SCA-GTS coating compared to SCA-GTS-Ce and SCA-GTS-Li coating [45,73].

After 28 d of immersion, the equivalent circuit of stand-alone SCA anodic film (Fig. 6a). This circuit includes the additional CPE_{pw} element, which is associated with the capacitive response of the pore walls due to their gradual degradation with time [49]. For SCA HSG-coated specimens, CPE_{GTS}/R_{GTS} represent the outer sol-gel coating and CPE_b/R_b the mixed anodic barrier layer (Fig. 6b) [76–78]. On that basis, all specimens reveal a slight decrease of the barrier properties (R_{GTS} , R_{hl} and R_b) due to the gradual electrolyte penetration throughout the GTS structure (Table 4) [46,73]. Note that the long-term corrosion improvement after Ce and Li addition during HSG formation was negligible. This could be related to the adverse effect of Li and Ce on the structural integrity of the pristine HSG layer, possibly related to the HSG formulation used in the present work, since in accordance with previous studies the presence of Ce and Li during HSG formation tends to increase the corrosion resistance [45,46,66,68,71].

Interestingly, CPE_{GTS} and CPE_b values of SCA-GTS-Li and SCA-GTS coatings were higher after the long-term immersion period. On the contrary, SCA-GTS-Ce showed practically constant CPE_{GTS} and CPE_b values. This suggests a lower coating permeability after the incorporation of Ce into the GTS formulation [68,71,73]. Present findings reveal the beneficial effect of Ce incorporation into GTS formulation in the long-term HSG coating stability.

HSG-coated specimens were analyzed by SEM (Fig. 7) and EDS analysis (Table 5) to ascertain the coating stability after the Ce- and Li incorporation into the HSG coating formulation. SCA film was not included in this test due to its low corrosion resistance.

SCA-GTS coating surface reveals numerous bright deposits and cracks (Fig. 7a, b), thus confirming the abovementioned lower GTS coating stability observed in EIS tests. These bright deposits revealed a high content of aluminium and oxygen (marked as 5 in Fig. 7a), indicating the possible formation of aluminium (hydr)oxides as corrosion products from the deterioration of the inner coating layers, i.e. SCA oxide film. The higher corrosion resistance provided by the SCA-GTS coating can be attributed to the passive character of these possible aluminium-based compounds [45,79].

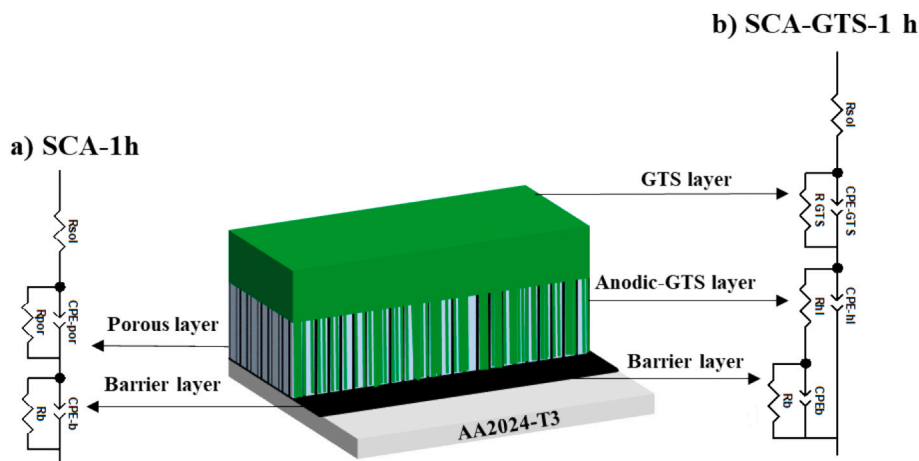


Fig. 5. Equivalent circuits used to fit the experimental EIS data for (a) stand-alone SCA film and (b) SCA-GTS coatings after 1 h of immersion in 0.1 mol L⁻¹ NaCl solution.

Table 4Fitted electrical parameters of studied coatings after 1 h and 28 days of immersion in 0.1 mol L⁻¹ NaCl solution.

Coating	R_{GTS} (Ωcm^2)	CPE_{GTS} ($\mu\text{F cm}^{-2} \text{s}^{(n-1)}$)	n_{GTS}	R_{hl} (Ωcm^2)	CPE_{hl} ($\mu\text{F cm}^{-2} \text{s}^{(n-1)}$)	n_{hl}	R_b/R_{por} (Ωcm^2)	CPE_b/CPE_{por} ($\mu\text{F cm}^{-2} \text{s}^{(n-1)}$)	CPE_w ($\mu\text{F cm}^{-2} \text{s}^{(n-1)}$)	n_b/n_{por}
1 h of immersion										
SCA	—	—	—	—	—	—	$7 \cdot 10^5/10^2$	0.6/0.1	—	0.9/0.8
SCA-GTS	$3 \cdot 10^4$	0.04	0.86	$2 \cdot 10^6$	0.21	0.92	$2.5 \cdot 10^7$	0.28	—	0.88
SCA-GTS-Li	$1 \cdot 10^3$	0.04	0.96	$3.5 \cdot 10^4$	0.17	0.93	$9.0 \cdot 10^6$	0.23	—	0.89
SCA-GTS-Ce	$2 \cdot 10^3$	0.05	0.98	$1.6 \cdot 10^5$	0.13	0.92	$9.4 \cdot 10^6$	0.21	—	0.92
28 days of immersion										
SCA	—	—	—	—	—	—	$7 \cdot 10^4/10$	0.7	0.1	0.6/0.4
SCA-GTS	$4 \cdot 10^4$	0.08	0.88	—	—	—	$2.0 \cdot 10^7$	0.87	—	0.97
SCA-GTS-Li	$1.5 \cdot 10^3$	0.04	0.91	—	—	—	$8.7 \cdot 10^6$	0.62	—	0.88
SCA-GTS-Ce	$5 \cdot 10^4$	0.04	0.86	—	—	—	$9.0 \cdot 10^6$	0.18	—	0.88

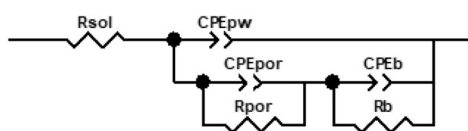
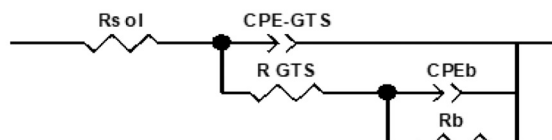
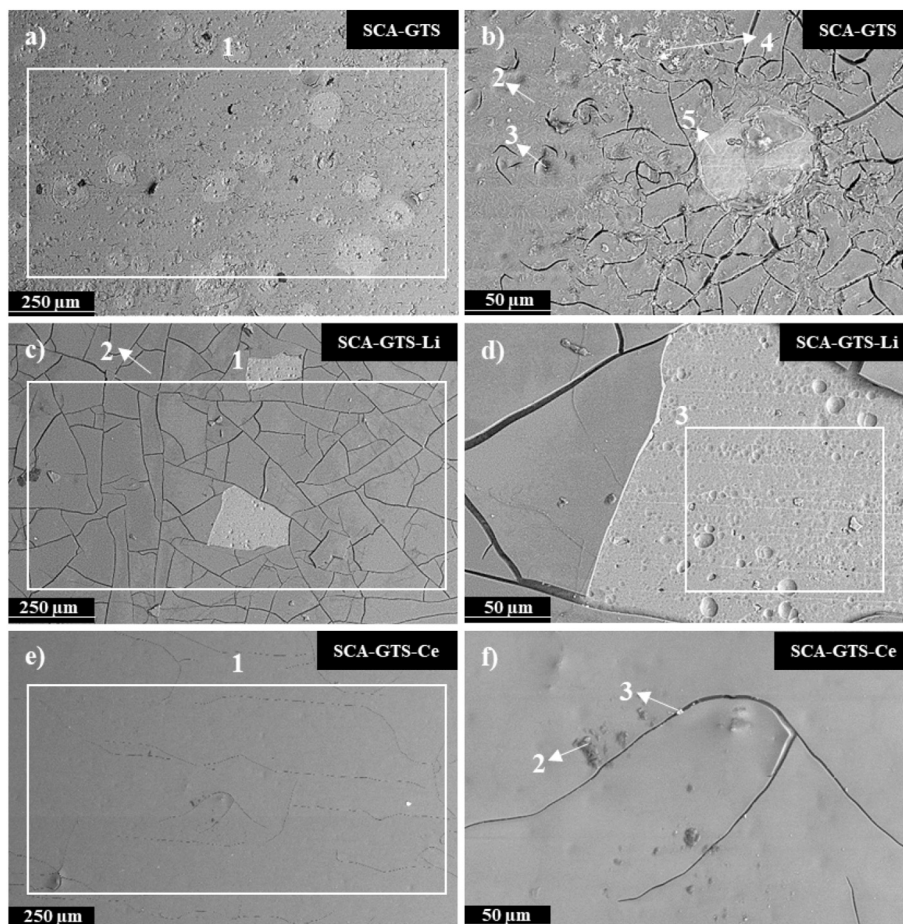
a) SCA-28d**b) SCA-GTS-28d****Fig. 6.** Equivalent circuits used to fit the experimental EIS data for (a) stand-alone SCA anodic film and (b) SCA-GTS coatings after 28d of immersion in 0.1 mol L⁻¹ NaCl solution.**Fig. 7.** Top-view scanning electron micrographs of (a,b) SCA-GTS, (c, d) SCA-GTS-Li, and (e, f) SCA-GTS-Ce, after 28 days immersion in 0.1 mol L⁻¹ NaCl solution.

Table 5

EDS analysis of SCA-GTS, SCA-GTS-Li and SCA-GTS-Ce coatings after 28 days of immersion in 0.1 mol L⁻¹ solution (at.%). Locations are denoted on the top-view SEM micrographs in Fig. 7.

Coating	Location	C	O	Al	S	Si
SCA-GTS	1	29.7	51.5	2.0		16.8
	2	23.0	56.0	1.4		19.6
	3	31.1	44.6	1.2		23.1
	4	17.3	55.8	16.5	1.7	8.7
	5	27.5	49.1	1.6		21.8
SCA-GTS-Li	1	36.3	47.5			16.2
	2	36.8	47.2	0.3		15.7
	3	21.4	55.3	15.9	1.3	6.1
SCA-GTS-Ce	1	37.1	47.5	0.2		15.2
	2	68.3	27.6			4.1
	3	37.7	45.2	0.4		16.7

Similarly, SCA-GTS-Li coating (Fig. 7c, d) showed a cracked surface and partial coating detachment during the corrosion process. EDS analysis (marked as 3 in Fig. 7d) showed S in the detached areas, indicating that the SCA film remains on the surface (Table 5).

The lower physical stability of Li-containing GTS coating in this study could be to some extent due to the HSG formulation. Also, the relatively low curing temperature and the high concentration of Li in this study could result in low diffusion of aluminium species from the SCA, thereby compromising the physical stability of the top-layer. This partial coating detachment may be in agreement with the Nyquist plot after 28 days of immersion (Fig. 4f) since the more resistive response of SCA-GTS-Li and SCA-GTS-Ce coatings may be associated with lower coating degradation in comparison to the SCA-GTS coating. Besides, the diffusion processes can be related to the observed cracked surface in both inhibitor-containing HSG coatings. Nonetheless, according to the EIS data and SEM examination, there is no damage of the underlying AA2024-T3 substrate.

Conversely, a much lesser cracked surface and no coating detachment was observed for the SCA-GTS-Ce coating, thus confirming its high stability during the corrosion process, as observed in the EIS test. This is in accordance with previous studies where Ce(NO₃)₃ addition favours the condensation and polymerization of both inorganic and organic networks of the hybrid sol-gel coating, which results in improved coating stability [36,80].

3.3. Characterization and corrosion behavior of scribed samples

Although Li and Ce addition in HSG tends to slightly decrease the impedance modulus values as compared to those of the stand-alone SCA-GTS coating, the influence of these species on the active corrosion protection ability of anodic/HSG duplex system when the damage occurs remains undisclosed. Hereto, SCA-GTS-Ce and SCA-GTS-Li scribed specimens were exposed in 0.5 mol L⁻¹ NaCl solution to accelerate the corrosion process and analyze the corrosion products and damage propagation by SEM/EDS and EIS (Fig. S1). The inhibitor-free SCA-GTS coating was also analyzed for comparison.

3.3.1. Immersion test of SCA-HSG coatings

Fig. 8 shows the digital micrographs of the scribed GTS-coated specimens in 0.5 mol L⁻¹ NaCl solution as a function of immersion time. SCA-GTS coating reveals several corrosion locations after three days of immersion and with the scribe width increasing due to corrosion products formation (Fig. 8a). Corrosion of the SCA-GTS-Li coating was observed after just one day of immersion, spreading over the whole scribed surface after three days of immersion (Fig. 8b). Conversely, SCA-GTS-Ce coating reveals several corrosion locations after three days, whereas the corrosion products were not observed till after seven days of immersion (Fig. 8c).

Compared to other studies on the AA2024-T3 sample coated with Li- [45], Ce- [68] and both-containing [30] HSG coatings, the present GTS-

coated specimens show better corrosion resistance at the scribed surface. This corrosion protection improvement was possibly due to the presence of the SCA anodic layer and a possible active corrosion protection ability, especially in the case of the SCA-GTS-Ce coating.

3.3.2. Evaluation of the active corrosion protection of scribed samples

Fig. 9 shows the evolution of corrosion damage on scribed SCA-GTS, SCA-GTS-Li and SCA-GTS-Ce specimens up to 21 days of immersion in 0.5 mol L⁻¹ NaCl solution. The EDS analysis of the studied GTS-coated specimens surface (Table 6) reveals that the concentration of C and Al decreased, whereas the O concentration increased at longer immersion times. This may be related to the simultaneous coating degradation and formation of Al (hydr)oxide compounds at the scribe [68]. For both SCA-GTS and SCA-GTS-Li coatings, the concentration of Si from the sol-gel part decreased as a function of immersion time (Table 6) due to progressive GTS coating dissolution [36,68].

Regardless of the inhibitor type, the addition of Li or Ce delays the coating cracking and peeling (Fig. 9b). For instance, SCA-GTS coating reveals a cracked surface and partial peeling after three days of immersion (Fig. 9a) due to its low post-damage stability. Conversely, SCA-GTS-Li coatings reveal a less cracked surface than SCA-GTS coating after three days of immersion, and the partial peeling did not occur till 14 days of immersion (Fig. 9b).

The less cracked surface is attributed to the presence of Li in the GTS structure. This is in agreement with previous studies where the active corrosion protection ability of Li-containing HSG, polyurethane and epoxy coatings has been demonstrated due to Li ion leaching to the damaged zone [38,40,41]. It should be noted that these above-mentioned Li-based salts (e.g Li₂CO₃, LiOH) were insoluble in the HSG solution used in the present work (GTS), forming white precipitates.

In the present study, the incorporation of a less alkaline salt (LiNO₃; pH: 4) into GTS formulation was beneficial, although the active protection mechanism is still under investigation.

For SCA-GTS-Ce coating, only a minor extent of surface cracking was observed after 14 days of immersion (Fig. 9c). Also, SCA-GTS-Ce coating peeling next to the scribe was not observed till 21 days of immersion. Besides, the Si concentration was practically constant during the full duration of immersion, denoting a higher coating stability during corrosive exposure (Table 6). This performance may be related to the preferential incorporation of Ce into the inner sol-gel layer, permeating the top region of SCA (designated as the SCA-GTS layer in Fig. 4) [73,81] and its possible release when the corrosion process occurs on a scribed surface.

To ascertain the compositional changes in the scribed area, Table 7 represents the EDS analysis on the scribes of the different GTS-coated specimens (Fig. 9) as a function of immersion time.

In all studied SCA-GTS coatings, Si and C were detected only outside the scribe, which is consistent with the undamaged GTS coating. Inside the scribe Al and Cu from the AA2024-T3 substrate were identified. The Cu signal vanishes by the formation of overlaying (hydr)oxides during immersion as revealed by the increased O content in the scribed area. S corresponding to the SCA film was detected in regions where the HSG top layer was delaminated.

In the particular case of SCA-GTS-Ce coating, a considerable amount of Ce (~4–5 at.%) was detected in the scribe after 3 days of immersion which remained relatively constant at longer immersion times (Table 7). The amount of Ce found in the deposits is much higher than that previously reported by Tiringier et al. [68] using the same sol-gel coating on a non-anodized AA7075-T6 (0.1–0.3 at.%), indicating that the presence of the SCA underlayer is an efficient Ce reservoir that facilitates its liberation.

The presence of Ce-rich deposits is associated with an active corrosion protection mechanism where Ce species leach from the coating and precipitate on the surface of cathodic sites [34].

Fig. 10 depicts a schematic illustration of the SCA-GTS-Ce coating and its corrosion protection mechanism. This mechanism is based on the

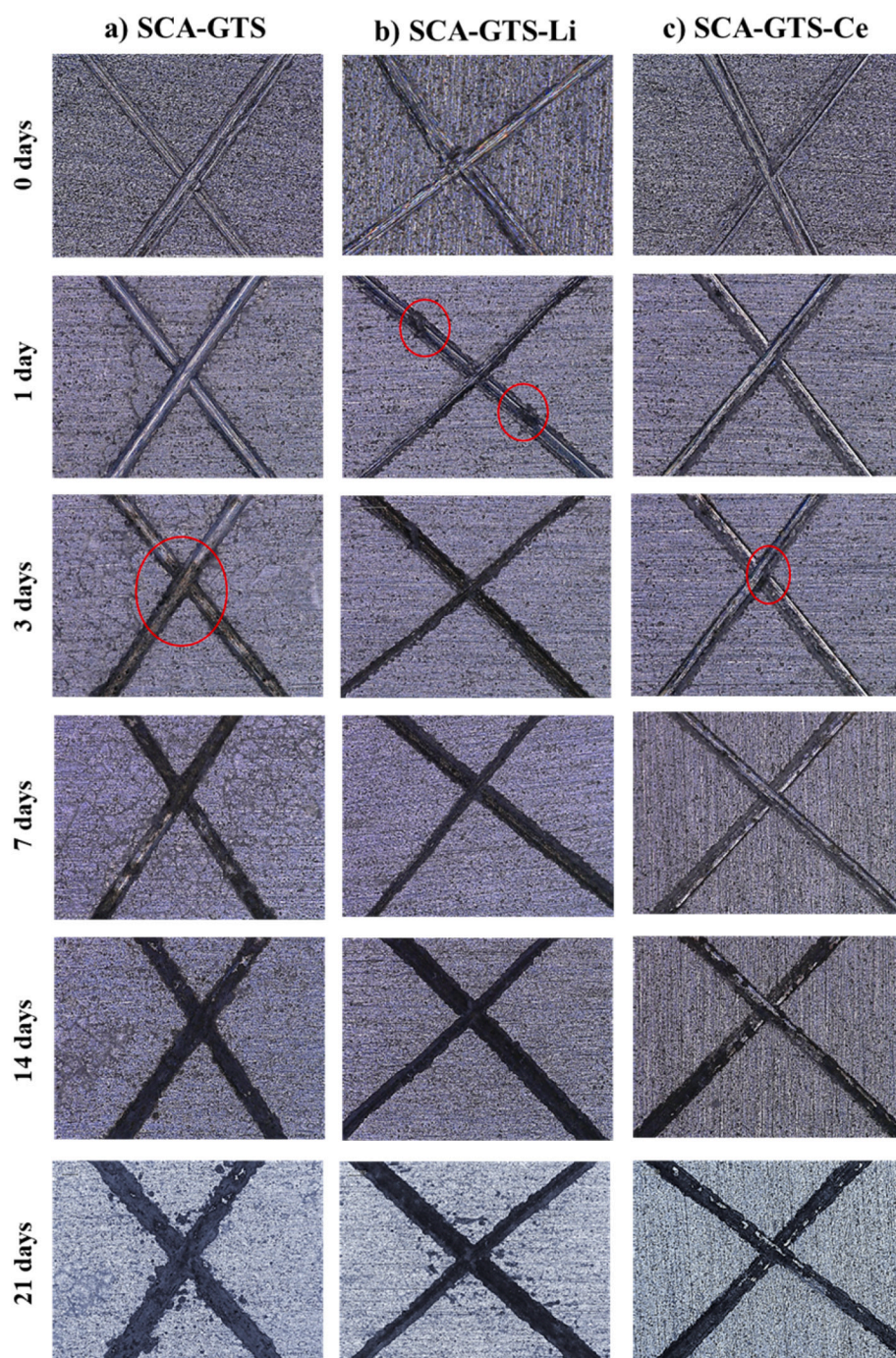


Fig. 8. Digital microscopy images of (a) SCA-GTS, (b) SCA-GTS-Li and (c) SCA-GTS-Ce scribed coatings during the immersion test in 0.5 mol L⁻¹ NaCl solution. Red circles indicate the visually observable onset of significant corrosion damage.

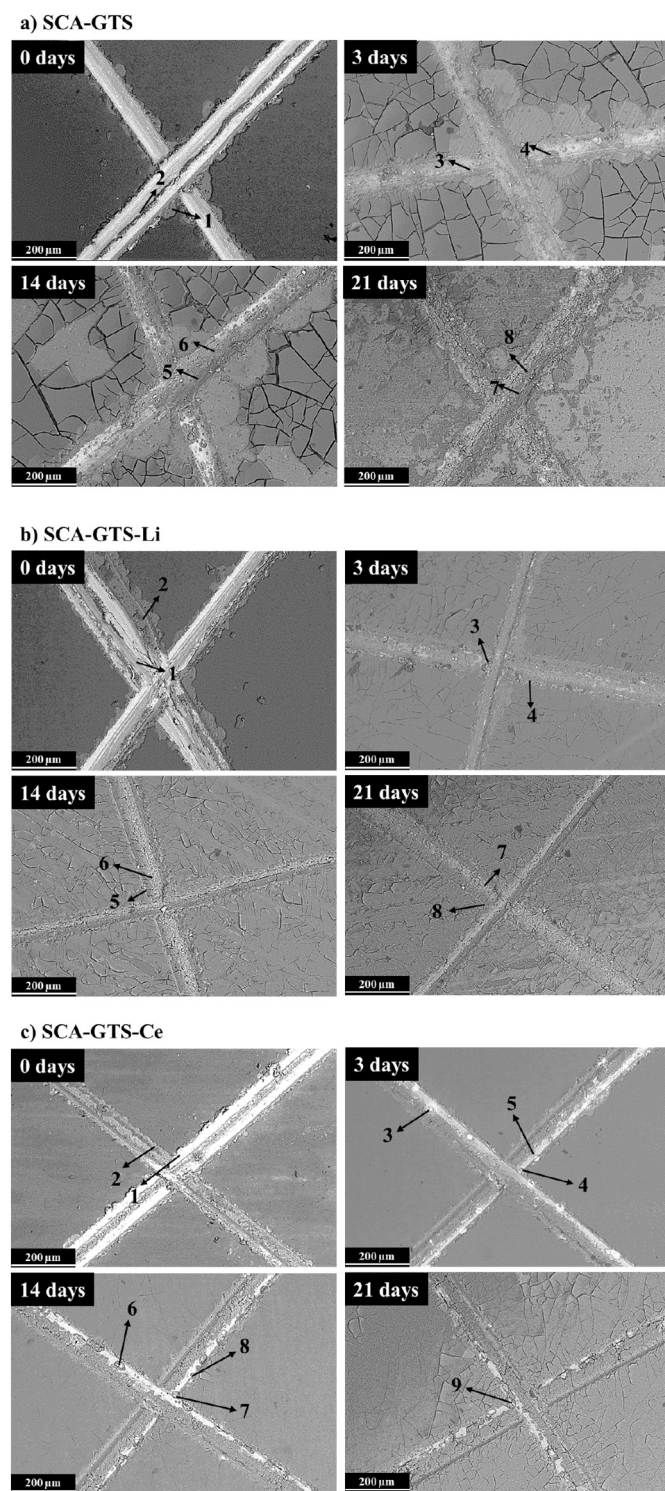


Fig. 9. Scanning electron micrographs corresponding to the scribed plan views of (a) SCA-GTS, (b) SCA-GTS-Li and (c) SCA-GTS-Ce coatings, before (0 days) and after 3, 14 and 28 days immersion in 0.5 mol L⁻¹ NaCl solution.

obtained results in this work and those obtained by Lakshmi et al. [81].

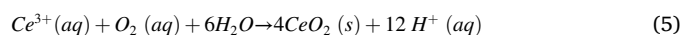
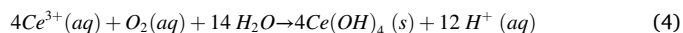
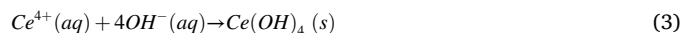
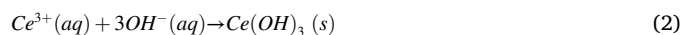
According to this mechanism, Ce soluble species leach from the coating. At this stage the majority of Ce is released as Ce³⁺, however some Ce⁴⁺ aqueous species are likely to be present as suggested by the pale yellow colour observed during the Ce-containing sol-gel synthesis (the use of HNO₃ during the synthesis may oxidize some Ce³⁺ into Ce⁴⁺ [81]). Then, precipitation of Ce (hydr)oxides takes place at the locations of intermetallic particles where the cathodic reaction is occurring (Eq.

Table 6

EDS analysis of the entire scribed coatings surface of SCA-GTS, SCA-GTS-Li and SCA-GTS-Ce coatings as a function of immersion time in 0.5 mol L⁻¹ NaCl solution (Fig. 9).

Coating	Days	C	O	Mg	Al	S	Si	Ce
SCA-GTS	0	36.5	40.9	0.3	11.6	–	10.7	–
	3	30.2	49.2	–	9.5	–	11.1	–
	14	20.8	57.6	0.2	13.6	1.1	6.7	–
	21	20.4	58.6	–	14.6	1.3	5.1	–
SCA-GTS-Li	0	32.1	42.2	0.4	13.7	0.4	11.2	–
	3	29.7	52.3	–	4.6	–	13.4	–
	14	27.0	52.8	0.1	7.9	0.7	11.5	–
	21	23.7	57.4	–	8.8	–	10.1	–
SCA-GTS-Ce	0	32.1	45.1	–	10.9	0.6	11.3	–
	3	32.2	48.1	–	7.5	–	12.2	0.3
	14	31.8	49.8	–	6.0	–	12.4	0.3
	21	27.31	55.17	–	5.74	–	11.54	0.24

(1)). In a neutral environment and in the presence of oxygen the dominant precipitates should be Ce(OH)₃ and Ce(OH)₄ [82] formed by the reactions indicated in Eq. (2), (3). Note that the precipitation of Ce(OH)₄ may occur either directly from the Ce(IV) present in the solution or from oxidation of Ce³⁺ as shown in (Eq. (4)) [82]. The precipitation of some CeO₂ is also possible according to (Eq. (5)), although the amount of this product should be negligible for the studied conditions



According to several studies, there is the risk that Ce salts are quickly released from HSG coatings into the damaged area, thereby leading to short-term inhibition followed by fast system degradation [83,84]. This issue is not observed in the SCA-GTS-Ce since Ce concentration on the cathodic sites was still high even after long immersion times (Table 7). Also, the coating remained intact in the unscribed regions without signs of degradation.

4. Conclusions

The main conclusions regarding the synthesis and application of inhibitor-free, Li- and Ce-loaded HSG coatings can be summarized as follows:

- The GTS formulations of the HSG coating (inhibitor-free, Li- and Ce-containing) were successfully synthesized and applied on the selected SCA-coated AA2024-T3.
- EIS measurements show the impedance modulus of SCA film to increase an order of magnitude after the GTS sol-gel application.
- In situ incorporation of Ce and Li into GTS formulation improved the coating stability and resulted in less degradation of the coatings in comparison to that of the SCA-GTS coating.
- Active corrosion protection is demonstrated by both SCA-GTS-Li and SCA-GTS-Ce coatings. Corrosion testing with scribed specimens revealed an improved performance of inhibitor-containing HSG coatings. The mechanism of Li inhibition was not elucidated due to the difficulties associated with the detection of this element. In case of Ce, it was demonstrated that the active corrosion protection provided by the coating was due to the release of Ce³⁺ species from the coating and the subsequent formation of Ce-based (hydr)oxides at coating defects.

Table 7

EDS analysis at the scribe at various locations (marked in Fig. 9) of SCA-GTS, SCA-GTS-Li and SCA-GTS-Ce coatings (at.%) as a function of immersion time in 0.5 mol L⁻¹ NaCl solution.

Coating	Days	Location	C	O	Al	S	Cu	Si	Ce
SCA-GTS	0	1	15.0	55.2	23.8	2.1		3.9	
		2	37.4	29.5	24.3		1.0	7.8	
	3	3	15.6	41.5	32.3		3.9	6.7	
		4	17.0	33.0	45.4		1.0	3.6	
	14	5	21.3	56.9	11.2			10.6	
		6	37.1	59.5	1.1			2.3	
	21	7		66.8	24.7	3.1		5.4	
		8		74.7	20.7			4.6	
SCA-GTS-Li	0	1		15.0	79.7		1.7	3.6	
		2	18.9	57.7	17.3	1.6		4.5	
	3	3	18.6	36.8	38.2			6.4	
		4	15.5	60.9	13.6			10.0	
	14	5	24.7	51.5	16.7			7.1	
		6	13.1	62.7	19.4			4.8	
	21	7	8.8	69.3	16.4			5.5	
		8	14.7	65.2	12.8			7.3	
SCA-GTS-Ce	0	1	22.7	9.3	64.2		1.5	2.3	
		2	15.6	55.5	22.7	2.6	0.6	3.0	
	3	3	16.6	48.6	23.2			7.4	4.2
		4	17.5	47.8	21.0			8.6	5.1
		5	20.8	54.4	13.7			7.4	3.7
	14	6	15.5	60.0	18.0			4.4	2.1
		7	12.9	63.5	16.3			4.9	2.4
		8	15.5	56.4	18.2			6.2	3.7
	21	9	18.7	53.6	15.4			8.0	4.3

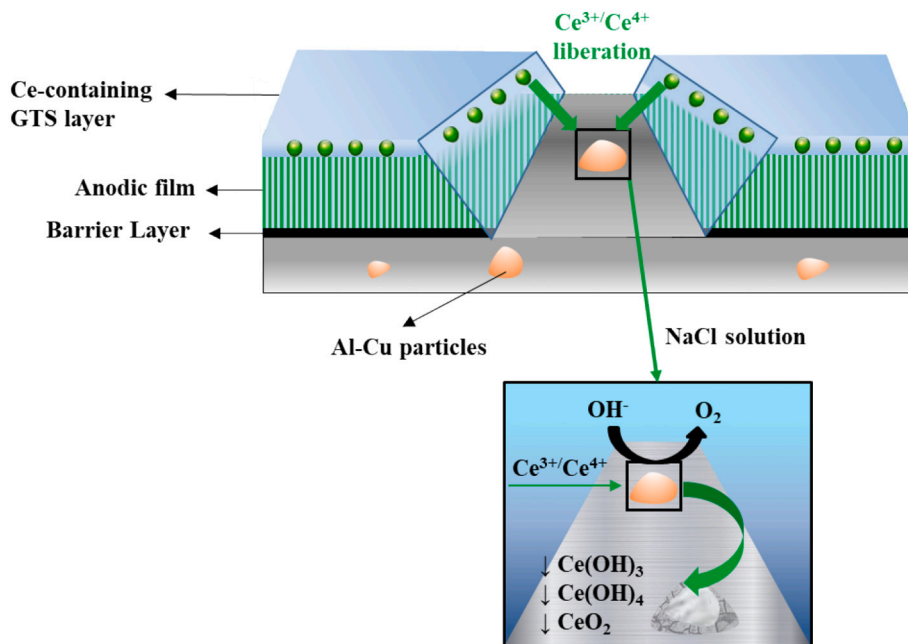


Fig. 10. Schematic illustration for active protection mechanism of SCA-GTS-Ce coating.

Present findings are highly relevant since SCA-GTS-Ce and SCA-GTS-Li coatings could be considered as a potential hexavalent chromium-free system for non-painted components in the aircraft industry. Nevertheless, more studies concerning mechanical performance, active protection and up-scaling should be carried out in the future.

CRediT authorship contribution statement

Ruben del Olmo: Conceptualization, Methodology, Experimental part, Writing- Original draft preparation.

Ursa Tiringier: Conceptualization, Methodology, Experimental part, Writing, Revision- Original draft preparation.

Ingrid Milošev: Writing- Reviewing and Editing.

Peter Visser: Conceptualization, Industrial based feedback, Reviewing.

Raúl Arrabal Durán: Supervision, Writing- Reviewing and Editing.

Endzhe Matykina: Supervision, Writing- Reviewing and Editing.

Arjan Mol: Supervision, Writing- Reviewing and Editing.

Acknowledgements/funding

The authors gratefully acknowledge the support of the RTI2018-096391-B-C33 (MCIU/AEI/FEDER, UE), ADITIMAT-CM (S2018/NMT-4411, Regional Government of Madrid and EU Structural and Social

Funds) and The European Union's Horizon 2020 research and innovation programme under the Marie Skłodowska-Curie grant agreement No. 707404. The authors gratefully acknowledge the technical support of Agnieszka Kooijman. The authors also acknowledge the measurements support of Shuai He.

Data statement

The raw/process data required to reproduce these findings cannot be shared at this time as the data also forms part of an ongoing study.

Declaration of competing interest

The authors declare that they have no known competing financial interests or personal relationships that could have appeared to influence the work reported in this paper.

References

- [1] A.P. Mouritz, 8 - aluminium alloys for aircraft structures, in: A.P. Mouritz (Ed.), *Introduction to Aerospace Materials*, Woodhead Publishing, 2012, pp. 173–201.
- [2] M.G.S. Ferreira, M.L. Zheludkevich, J. Tedim, *Advanced Protective Coatings for Aeronautical Applications, Nanocoatings and Ultra-thin Films, Technologies and Applications*, 2011, pp. 235–279.
- [3] P. Visser, H. Terryn, J.M.C. Mol, *Aerospace coatings*, in: *Springer Series in Materials Science*, 2016, pp. 315–372.
- [4] LANXESS, *Surface Treatment for Applications in the Aeronautics and Aerospace Industries, Analysis of Alternatives, Non-confidential Report*, Available from: <http://echa.europa.eu/es/support/substance-identification>, 2018, p. 137.
- [5] R.L. Twite, G.P. Bierwagen, Review of alternatives to chromate for corrosion protection of aluminum aerospace alloys, *Prog. Org. Coat.* 33 (1998) 91–100.
- [6] O. Gharbi, S. Thomas, C. Smith, N. Biribilis, Chromate replacement: what does the future hold? *npj Mater. Degrad.* 2 (2018) 12.
- [7] M. Becker, Chromate-free chemical conversion coatings for aluminum alloys, *Corros. Rev.* 37 (2019) 321–342.
- [8] S.T. Abrahami, J.M.M. de Kok, H. Terryn, J.M.C. Mol, Towards Cr(VI)-free anodization of aluminum alloys for aerospace adhesive bonding applications: a review, *Front. Chem. Sci. Eng.* 11 (2017) 465–482.
- [9] Use of potassium dichromate for sealing after anodizing applications by aerospace companies and their suppliers, 2018, Available from: <https://echa.europa.eu/documents/10162/d6c88cd1-ef18-460b-8493-ed59211a888>, Haas Group International, pp. 65.
- [10] K. Barton, M. Cullen, B. Duffy, Sol-gel chemistry engineering for corrosion protection, in: *Sol-gel Materials for Energy, Environment and Electronic Applications*, 2017, pp. 197–241.
- [11] L.G. Ecco, M. Fedel, F. Deflorian, J. Becker, B.B. Iversen, A. Mamakhel, Waterborne acrylic paint system based on nanoceria for corrosion protection of steel, *Prog. Org. Coat.* 96 (2016) 19–25.
- [12] M. Paz Martínez-Viademonte, S.T. Abrahami, T. Hack, M. Burchardt, H. Terryn, A Review on Anodizing of Aerospace Aluminum Alloys for Corrosion Protection 10, 2020, p. 1106.
- [13] Z. Ding, B.A. Smith, R.R. Hebert, W. Zhang, M.R. Jaworowski, Morphology perspective on chromic acid anodizing replacement by thin film sulfuric acid anodizing, *Surf. Coat. Technol.* 350 (2018) 31–39.
- [14] J.M. Runge, *The Metallurgy of Anodizing Aluminium*, Springer Nature, 2018.
- [15] A. Yerokhin, R.H.U. Khan, 4 - anodising of light alloys, in: H. Dong (Ed.), *Surface Engineering of Light Alloys*, Woodhead Publishing, 2010, pp. 83–109.
- [16] M.E.N. Beck, Performance Validation of Thin-film Sulfuric Acid Anodization (TFSAA) on Aluminum Alloys, Naval Air Systems Command (NAVAIR), 2003.
- [17] R. Giovanardi, C. Fontanesi, W. Dallabarra, Adsorption of organic compounds at the aluminium oxide/aqueous solution interface during the aluminium anodizing process, *Electrochim. Acta* 56 (2011) 3128–3138.
- [18] T. Kikuchi, D. Nakajima, O. Nishinaga, S. Natsui, R. Suzuki, Porous aluminum oxide formed by anodizing in various electrolyte species, *Curr. Nanosci.* 11 (2015).
- [19] A.E. Koczera, The Effects of Carboxylic Acids in Aluminum Anodizing University of New Hampshire, 2017, p. 330.
- [20] T. Vignoli Machado, P. Atz Dick, G.H. Knörschild, L.F.P. Dick, The effect of different carboxylic acids on the sulfuric acid anodizing of AA2024, *Surf. Coat. Technol.* 383 (2020), 125283.
- [21] M. Xiangfeng, G. Wei, G. Hongliang, Y. Yundan, C. Ying, H. Dettinger, Anodization for 2024 Al alloy from sulfuric-citric acid and anticorrosion performance of anodization films, *Int. J. Electrochem. Sci.* 8 (2013) 10660–10671.
- [22] H. Jalal, Y. Saoud, F. Karabet, Effect of organic additives on AA6066 anodization, *J. Chem. Technol. Metall.* 54 (2019) 447–453.
- [23] R.B. Figueira, Hybrid sol-gel coatings for corrosion mitigation: a critical review, *Polymers* 12 (2020) 689.
- [24] R. Figueira, C. Silva, E. Pereira, Organic-inorganic hybrid sol-gel coatings for metal corrosion protection: a review of recent progress, *J. Coat. Technol. Res.*, <https://doi.org/10.1007/s11998-014-9595-6> (2014).
- [25] C.J. Brinker, G.W. Scherer, CHAPTER 10 - surface chemistry and chemical modification, in: C.J. Brinker, G.W. Scherer (Eds.), *Sol-Gel Science*, Academic Press, San Diego, 1990, pp. 616–672.
- [26] S. Zheng, J. Li, Inorganic-organic sol gel hybrid coatings for corrosion protection of metals, *J. Sol-Gel Sci. Technol.* 54 (2010) 174–187.
- [27] J. Wen, G.L. Wilkes, Organic/inorganic hybrid network materials by the sol-gel approach, *Chem. Mater.* 8 (1996) 1667–1681.
- [28] D. Balgude, A. Sabnis, Sol-gel derived hybrid coatings as an environment friendly surface treatment for corrosion protection of metals and their alloys, *J. Sol-Gel Sci. Technol.* 64 (2012) 124–134.
- [29] H. Wang, R. Akid, Encapsulated cerium nitrate inhibitors to provide high-performance anti-corrosion sol-gel coatings on mild steel, *Corros. Sci.* 50 (2008) 1142–1148.
- [30] S. He, Lithium and Cerium Based Sol-Gel Coatings for Corrosion Protection of AA2024-T3, Delft University of Technology, 2020.
- [31] A. Galio, C. Dariva, *Corrosion Inhibitors – Principles, Mechanisms and Applications*, 2014, pp. 365–380.
- [32] G. Yoganandan, K. Pradeep Premkumar, J.N. Balaraju, Evaluation of corrosion resistance and self-healing behavior of zirconium-cerium conversion coating developed on AA2024 alloy, *Surf. Coat. Technol.* 270 (2015) 249–258.
- [33] W. Trabelsi, P. Cecilio, M.G.S. Ferreira, M.F. Montemor, Electrochemical assessment of the self-healing properties of Ce-doped silane solutions for the pre-treatment of galvanised steel substrates, *Prog. Org. Coat.* 54 (2005) 276–284.
- [34] K.A. Yasakau, M.L. Zheludkevich, S.V. Lamaka, M.G.S. Ferreira, Mechanism of corrosion inhibition of AA2024 by rare-earth compounds, *J. Phys. Chem. B* 110 (2006) 5515–5528.
- [35] A.J. Aldykiewicz, A.J. Davenport, H.S. Isaacs, Studies of the formation of cerium-rich protective films using X-ray absorption near-edge spectroscopy and rotating disk electrode methods, *J. Electrochem. Soc.* 143 (1996) 147–154.
- [36] U. Tiringir, B. Musić, D. Zimerl, G. Sekularac, S. Stavber, I. Milošev, The effects of cerium ions on the curing, polymerisation and condensation of hybrid sol-gel coatings, *J. Non-Cryst. Solids* 510 (2019) 93–100.
- [37] P. Visser, H. Terryn, J.M.C. Mol, Active corrosion protection of various aluminium alloys by lithium-leaching coatings, *Surf. Interface Anal.* 51 (2019) 1276–1287.
- [38] P. Visser, M. Meeusen, Y. Gonzalez-Garcia, H. Terryn, J.M.C. Mol, Electrochemical evaluation of corrosion inhibiting layers formed in a defect from lithium-leaching organic coatings, *J. Electrochem. Soc.* 164 (2017) 396–406.
- [39] P. Visser, K. Marcoen, G.F. Trindade, M.L. Abel, J.F. Watts, T. Hauffman, J.M. C. Mol, H. Terryn, The chemical throwing power of lithium-based inhibitors from organic coatings on AA2024-T3, *Corros. Sci.* 150 (2019) 194–206.
- [40] P. Visser, Y. Liu, X. Zhou, T. Hashimoto, G.E. Thompson, S.B. Lyon, L.G.J. van der Ven, A.J.M.C. Mol, H.A. Terryn, The corrosion protection of AA2024-T3 aluminium alloy by leaching of lithium-containing salts from organic coatings, *Faraday Discuss.* 180 (2015) 511–526.
- [41] P. Visser, Y. Liu, H. Terryn, J.M.C. Mol, Lithium salts as leachable corrosion inhibitors and potential replacement for hexavalent chromium in organic coatings for the protection of aluminium alloys, *J. Coat. Technol. Res.* 13 (2016) 1–10.
- [42] J. Gui, T.M. Devine, Influence of lithium on the corrosion of aluminum, *Scr. Metall.* 21 (1987) 853–857.
- [43] R. Buchheit, M. Bode, G. Stoner, Corrosion-resistant, chromate-free talc coatings for aluminum, *Corrosion* 50 (1994) 205–214.
- [44] P. Visser, A. Lutz, J.M.C. Mol, H. Terryn, Study of the formation of a protective layer in a defect from lithium-leaching organic coatings, *Prog. Org. Coat.* 99 (2016) 80–90.
- [45] A. Trentin, S.V. Harb, M.C. Uvida, S.H. Pulcinelli, C.V. Santilli, K. Marcoen, S. Pletincx, H. Terryn, T. Hauffman, P. Hammer, Dual role of lithium on the structure and self-healing ability of PMMA-silica coatings on AA7075 alloy, *ACS Appl. Mater. Interfaces* 11 (2019) 40629–40641.
- [46] M. Terada, F.M. Queiroz, D.B.S. Aguiar, V.H. Ayusso, H. Costenaro, M.G. Olivier, H.G. de Melo, I. Costa, Corrosion resistance of tartaric-sulfuric acid anodized AA2024-T3 sealed with Ce and protected with hybrid sol-gel coating, *Surf. Coat. Technol.* 372 (2019) 422–426.
- [47] H. Costenaro, A. Lanzutti, Y. Paint, L. Fedrizzi, M. Terada, H.G. de Melo, M. G. Olivier, Corrosion resistance of 2524 Al alloy anodized in tartaric-sulphuric acid at different voltages and protected with a TEOS-GPTMS hybrid sol-gel coating, *Surf. Coat. Technol.* 324 (2017) 438–450.
- [48] M. Whelan, E. Tobin, J. Cassidy, B. Duffy, Optimization of anodic oxidation of aluminum for enhanced adhesion and corrosion properties of sol-gel coatings, *J. Electrochem. Soc.* 163 (2016) C205–C212.
- [49] V.R. Capelossi, M. Poelman, I. Recloux, R.P.B. Hernandez, H.G. de Melo, M. G. Olivier, Corrosion protection of clad 2024 aluminum alloy anodized in tartaric-sulfuric acid bath and protected with hybrid sol-gel coating, *Electrochim. Acta* 124 (2014) 69–79.
- [50] S.M. Beden, S. Abdullah, A.K. Ariffin, N.A. Al-Asady, Fatigue crack growth simulation of aluminium alloy under spectrum loadings, *Mater. Des.* 31 (2010) 3449–3456.
- [51] Military Specification Anodic Coatings for Aluminum and Aluminum Alloys (MIL-A-8625F), Departments and Agencies of the Department of Defense, 1993.
- [52] G. Boisier, N. Pébère, C. Druez, M. Villatte, S. Suel, FESEM and EIS study of sealed AA2024 T3 anodized in sulfuric acid electrolytes: influence of tartaric acid, *J. Electrochem. Soc.* 155 (2008).
- [53] M. Curioni, P. Skeldon, E. Koroleva, G. Thompson, J. Ferguson, Role of tartaric acid on the anodizing and corrosion behavior of AA 2024 T3 aluminum alloy, *J. Electrochem. Soc.* 156 (2009) C147–C153.

- [54] A. Bodor, I. Bányai, L. Zékány, I. Tóth, Slow dynamics of aluminium-citrate complexes studied by ¹H- and ¹³C-NMR spectroscopy, *Coord. Chem. Rev.* 228 (2002) 163–173.
- [55] R.J. Motekaitis, A.E. Martell, Complexes of aluminum(III) with hydroxy carboxylic acids, *Inorg. Chem.* 23 (1984) 18–23.
- [56] Y. Ma, Y. Wen, J. Li, J. Lu, Y. Li, Y. Yang, C. Feng, C. Hao, Z. Zhang, J. Hu, R. Sun, Pore nucleation mechanism of self-ordered alumina with large period in stable anodization in citric acid, *J. Electrochem. Soc.* 165 (2018) E311–E317.
- [57] D.R. Lide, *CRC Handbook of Chemistry and Physics: A Ready-Reference of Chemical and Physical Data*, 85th ed., American Chemical Society, 2005.
- [58] S.J. García-Vergara, K. El Khazmi, P. Skeldon, G.E. Thompson, Influence of copper on the morphology of porous anodic alumina, *Corros. Sci.* 48 (2006) 2937–2946.
- [59] C. Girginov, S. Kozhukharov, M. Milanes, M. Machkova, Impact of the anodizing duration on the surface morphology and performance of AA2024-T3 in a model corrosive medium, *Mater. Chem. Phys.* 198 (2017) 137–144.
- [60] M. Arenas-Vara, P. Skeldon, S. García-Vergara, Effect of copper-enriched layers on localized corrosion of aluminium-copper alloys, *Revista Facultad de Ingeniería* 27 (2018).
- [61] B. Mingo, A. Němcová, D. Hamad, R. Arrabal, E. Matykina, M. Curioni, P. Skeldon, G. Thompson, Efficiency of anodizing of Al–Cu alloy in sulphuric acid at low potentials, *Trans. IMF* 93 (2015) 18–23.
- [62] M.A. van Put, S.T. Abrahams, O. Elisseeva, J.M.M. de Kok, J.M.C. Mol, H. Terryn, Potentiodynamic anodizing of aluminum alloys in Cr(VI)-free electrolytes, *Surf. Interface Anal.* 48 (2016) 946–952.
- [63] A. Wittmar, H. Caparrotti, M. Wittmar, M. Veith, Simple preparation routes for corrosion protection hybrid sol-gel coatings on AA 2024, *Surf. Interface Anal.* 44 (2012) 70–77.
- [64] N. Pirhady Tavandashti, S. Sanjabi, T. Shahrabi, Evolution of corrosion protection performance of hybrid silica based sol-gel nanocoatings by doping inorganic inhibitor, *Mater. Corros.* 62 (2011) 411–415.
- [65] M.J. Bartolomé, V. López, E. Escudero, G. Caruana, J.A. González, Changes in the specific surface area of porous aluminium oxide films during sealing, *Surf. Coat. Technol.* 200 (2006) 4530–4537.
- [66] J.-B. Cambon, J. Esteban, F. Ansart, J.-P. Bonino, V. Turq, S.H. Santagneli, C. V. Santilli, S.H. Pulcinelli, Effect of cerium on structure modifications of a hybrid sol-gel coating, its mechanical properties and anti-corrosion behavior, *Mater. Res. Bull.* 47 (2012) 3170–3176.
- [67] J. Gandhi, S. Singh, W.J.v. Ooij, P. Puomi, Evidence for formation of metallo-siloxane bonds by comparison of dip-coated and electrodeposited silane films, *J. Adhes. Sci. Technol.* 20 (2006) 1741–1768.
- [68] U. Tiringier, A. Durán, Y. Castro, I. Milošev, Self-healing effect of hybrid sol-gel coatings based on GPTMS, TEOS, SiO₂ nanoparticles and Ce(NO₃)₃ applied on aluminum alloy 7075-T6, *J. Electrochem. Soc.* 165 (2018) C213–C225.
- [69] J. Goldstein, D. Newbury, P. Echlin, D. Joy, C. Lyman, E. Lifshin, L. Sawyer, J. Michael, in: J. Goldstein (Ed.), *Scanning Electron Microscopy and X-ray Microanalysis*, Springer, Boston, 2003, pp. 591–619.
- [70] A. Lasia, *Electrochemical Impedance Spectroscopy and Its Applications*, 1999, pp. 143–248.
- [71] U. Tiringier, I. Milošev, A. Durán, Y. Castro, Hybrid sol-gel coatings based on GPTMS/TEOS containing colloidal SiO₂ and cerium nitrate for increasing corrosion protection of aluminium alloy 7075-T6, *J. Sol-Gel Sci. Technol.*, <https://doi.org/10.1007/s10971-017-4577-7> (2018).
- [72] L. Pausa, N.C. Rosero-Navarro, F. Andreatta, Y. Castro, A. Duran, M. Aparicio, L. Fedrizzi, Inhibition effect of cerium in hybrid sol-gel films on aluminium alloy AA2024, *Surf. Interface Anal.* 42 (2010) 299–305.
- [73] Y. Castro, E. Özmen, A. Durán, Integrated self-healing coating system for outstanding corrosion protection of AA2024, *Surf. Coat. Technol.* 387 (2020), 125521.
- [74] P.L. Bonora, F. Deflorian, L. Fedrizzi, Electrochemical impedance spectroscopy as a tool for investigating underpaint corrosion, *Electrochim. Acta* 41 (1996) 1073–1082.
- [75] V. Moutarlier, M.P. Gigandet, B. Normand, J. Pagetti, EIS characterisation of anodic films formed on 2024 aluminium alloy, in sulphuric acid containing molybdate or permanganate species, *Corros. Sci.* 47 (2005) 937–951.
- [76] T.T. Thai, M.E. Druart, Y. Paint, A.T. Trinh, M.G. Olivier, Influence of the sol-gel mesoporosity on the corrosion protection given by an epoxy primer applied on aluminum alloy 2024-T3, *Prog. Org. Coat.* 121 (2018) 53–63.
- [77] M.L. Zheludkevich, R. Serra, M.F. Montemor, K.A. Yasakau, I.M.M. Salvado, M.G. S. Ferreira, Nanostructured sol-gel coatings doped with cerium nitrate as pre-treatments for AA2024-T3: corrosion protection performance, *Electrochim. Acta* 51 (2005) 208–217.
- [78] T.T. Thai, A.T. Trinh, M.-G. Olivier, Hybrid sol-gel coatings doped with cerium nanocontainers for active corrosion protection of AA2024, *Prog. Org. Coat.* 138 (2020), 105428.
- [79] N.C. Rosero-Navarro, L. Pausa, F. Andreatta, Y. Castro, A. Durán, M. Aparicio, L. Fedrizzi, Optimization of hybrid sol-gel coatings by combination of layers with complementary properties for corrosion protection of AA2024, *Prog. Org. Coat.* 69 (2010) 167–174.
- [80] P. Rodič, I. Milošev, Corrosion Inhibition of Pure Aluminium and Alloys AA2024-T3 and AA7075-T6 by Cerium(III) and Cerium(IV) Salts, 2016.
- [81] R.V. Lakshmi, S.T. Aruna, C. Anandan, P. Bera, S. Sampath, EIS and XPS studies on the self-healing properties of Ce-modified silica-alumina hybrid coatings: evidence for Ce(III) migration, *Surf. Coat. Technol.* 309 (2017) 363–370.
- [82] P. Yu, S.A. Hayes, T.J. O'Keefe, M.J. O'Keefe, J.O. Stoffer, The phase stability of cerium species in aqueous systems, *J. Electrochem. Soc.* 153 (2006) C74.
- [83] J. De Damborenea, A. Conde, M.A. Arenas, Corrosion inhibition with rare earth metal compounds in aqueous solutions, in: *Rare Earth-based Corrosion Inhibitors*, 2014, pp. 84–116.
- [84] K. Barton, M. Cullen, B. Duffy, *Sol-Gel Chemistry Engineering for Corrosion Protection*, 2017, pp. 197–241.